

This document is confidential and is proprietary to the American Chemical Society and its authors. Do not copy or disclose without written permission. If you have received this item in error, notify the sender and delete all copies.

### **Dynamical Effects in Protein Electrochemistry**

Journal:	<i>The Journal of Physical Chemistry</i>
Manuscript ID	jp-2019-04516h.R2
Manuscript Type:	Article
Date Submitted by the Author:	n/a
Complete List of Authors:	Matyushov, Dmitry; Arizona State University, School of Molecular Sciences

SCHOLARONE™  
Manuscripts

# Dynamical Effects in Protein Electrochemistry

Dmitry V. Matyushov\*

*Department of Physics and School of Molecular Sciences, Arizona State University, PO Box*

*871504, Tempe, AZ 85287-1504*

E-mail: [dmitrym@asu.edu](mailto:dmitrym@asu.edu), Tel: (480)965-0057

## Abstract

Electrochemical measurements of electron transfer from an electrode to proteins immobilized at protective layers of varying thickness have shown the presence of two characteristic regimes: (i) exponential (tunneling) decay of the rate constant with the distance to the electrode and (ii) a plateau region where the rate is independent of the distance to the electrode. The reaction in the plateau region is viewed as friction-controlled electron transfer, with the rate constant inversely proportional to the medium relaxation time. Fitting the rates to established theories requires medium relaxation times far exceeding common estimates and relaxation times obtained from computer simulations of the Stokes-shift dynamics. There is a significant disconnect between experimental observations and theoretical expectations. This difficulty is resolved here by allowing additional dissipative dynamics consisting of protein's low-frequency oscillations in a soft harmonic potential describing binding of the protein to the substrate. Protein translational motions modulate the electrode-protein electronic coupling, leading to a new time-scale appearing, along with the Stokes-shift relaxation time, in the pre-exponential factor of the rate constant. The new model provides a consistent account of the experimental data. The anticipated range of friction-controlled kinetics is significantly extended since the effective relaxation time entering the rate pre-exponential factor gains an exponential dependence on the mean-square displacement of the protein. Since the mean-square displacement is proportional to temperature, the enthalpy of activation acquires a significant and non-trivial temperature dependence. The possibility of a negative reaction enthalpy is predicted.

## Introduction

Transport of electrons through chains of redox molecules (cofactors), usually immersed in the protein core, is fundamental for production of biological energy.<sup>1</sup> The protein matrix acts as a catalyst, i.e., it lowers the activation barrier for each elementary electron hop compared to the same reaction in bulk water.<sup>2</sup> The free energy of activation (activation barrier) is the reversible work to reorganize the medium to the tunneling configuration.<sup>3</sup> The free energy of activation is, in turn, affected by two free-energy parameters: the reaction free energy (the difference in free energies between the

1  
2  
3 products and reactants) and the reorganization energy (also a free energy). It is this latter free energy  
4 of medium reorganization that is dramatically reduced by the protein compared to solution to allow  
5 catalytic action.<sup>4</sup> The reaction free energy is of lesser significance for electron transfer in biology  
6 compared to many photoinduced electron-transfer reactions displaying the inverted-region behav-  
7 ior.<sup>5</sup> In contrast, biological electron transfer often occurs in the normal region, with a near-zero  
8 reaction free energy.<sup>1</sup> However, altering the free energy of a reaction is important for mechanis-  
9 tic studies of electron transfer,<sup>6</sup> and electrochemistry offers this opportunity through sweeping the  
10 electrode potential.<sup>7</sup> This control parameter makes this experimental tool very attractive to access  
11 mechanistic properties of protein electron transfer.<sup>8,9</sup> An additional advantage is the ability to di-  
12 rectly probe redox properties of the protein active site. This advantage comes in contrast to designs  
13 involving an electron donor attached to the surface of the protein.<sup>10</sup> The reorganization energy of  
14 electron transfer in these donor-acceptor systems is dominated by the non-native donor exposed to  
15 the water solvent.<sup>11</sup>

16  
17  
18  
19  
20  
21  
22  
23  
24  
25  
26  
27  
28  
29  
30  
31  
32  
33  
34  
35  
36  
37  
38  
39  
40  
41  
42  
43  
44  
45  
46  
47  
48  
49  
50  
Probability of electron tunneling between the active site of the protein and the electrode decays  
exponentially with the distance.<sup>12</sup> This information can be accessed by varying the thickness of  
the self-assembled monolayer (SAM) placed on the surface of the electrode.<sup>13,14</sup> Such a setup was  
applied to cytochrome and azurin metalloproteins at gold electrodes covered by alkenethiolates and  
indeed produced the anticipated exponential decay of the reaction rate with increasing thickness of  
the SAM.<sup>15-19</sup> However, the exponential falloff was observed only for sufficiently large distances,  
while the reaction rate plotted as a function of the SAM thickness was found to saturate to a plateau  
at shorter protein-electrode separations.<sup>15-20</sup> The possibility of gating, i.e., control of the reaction by  
conformational changes/reorientations at the surface of the monolayer,<sup>20-22</sup> was dismissed by recent  
measurements involving proteins bound to SAMs.<sup>18,19,23</sup> The current view favors the dynamic,  
friction-controlled origin of the reaction's crossover from an exponential decay to a plateau region.

51  
52  
53  
54  
55  
56  
57  
58  
59  
60  
The dynamic (friction control) explanation for the observed crossover invokes a general phe-  
nomenology of electron-transfer reactions affected by the solvent dynamics.<sup>24-28</sup> Theories of the  
solvent effect on electron transfer predict that even for a non-adiabatic reaction with the donor-

1  
2  
3 acceptor coupling  $V$  below  $k_{\text{B}}T$ ,<sup>29</sup> the dynamics of barrier crossing become affected by Kramers-  
4 type diffusion at the top of the activation barrier<sup>30</sup> if the medium is sufficiently slow. To reach this  
5 regime, the medium relaxation time has to exceed the time of electron tunneling in the activated  
6 state. More precisely, the condition of reaching the regime of dynamical control is determined by  
7 the dynamic crossover parameter  $g$ . It is given for an electrochemical reaction by the following  
8 relation (eq 37 in ref 31)  
9  
10  
11  
12  
13  
14

$$g \simeq 8\tau_x k_{\text{B}}T\Delta/(\hbar\lambda^r) \quad (1)$$

15  
16  
17 Here,  $\Delta = \pi V_{\mu}^2 \rho_{\mu}$  is the coupling strength between the reactant and the electrode. It is defined in  
18 terms of the electronic coupling  $V_{\mu}$  between the electronic state localized on the reactant and the  
19 conduction electronic states in the metal. Further,  $\rho_{\mu}$  is the density of electronic conduction states  
20 at the Fermi level,<sup>32</sup> and  $V_{\mu}$  refers to the coupling to the same Fermi-level states. Note that the  
21 crossover parameter in eq 37 in ref 31 involves the factor of 4 when diffusional mass transport to  
22 the electrode is considered. In contrast, a factor of 8 appears in eq 1 for the crossover parameter in  
23 the case of the surface-bound reactant.  
24  
25  
26  
27  
28  
29  
30  
31

32 In eq 1,  $\lambda^r$  is the effective “reaction” reorganization energy discussed below, which is distinct  
33 from the Marcus definition<sup>3</sup> and reflects nonergodic sampling of the configuration space available  
34 to the protein on the reaction time.<sup>4</sup> Finally,  $\tau_x$  is the average Stokes-shift relaxation time<sup>33</sup> repre-  
35 senting the decay of the time correlation function of the energy-gap collective reaction coordinate  
36  $X(t)$  defined below. The crossover to the solvent dynamical control occurs when  $g > 1$ , which  
37 requires a sufficiently slow decay of dynamical correlations for the nuclear medium modes coupled  
38 to the reaction coordinate  $X$  (large  $\tau_x$  in eq 1).  
39  
40  
41  
42  
43  
44  
45

46 A number of detailed experimental studies performed in recent years have resulted in a con-  
47 sistent phenomenology for the interfacial protein electron transfer.<sup>17–19,34,35</sup> These results can be  
48 summarized by the following key observations: (1) There is a crossover in the distance dependence  
49 of the reaction rate from an exponential decay at large protein-electrode distances to a plateau at  
50 shorter distances. (2) The apparent enthalpy of activation obtained from the Arrhenius plot sub-  
51 stantially increases in the plateau region.<sup>18,19,35</sup> The activation enthalpy  $\simeq \lambda^r/4$  predicted by the  
52  
53  
54  
55  
56  
57  
58  
59  
60

Marcus theory<sup>3</sup> is consistent with the independently measured reorganization energy  $\lambda^r$  at longer distances. (3) The volume of activation changes its sign from negative at long distances to positive at shorter distances, in parallel with an increase in the activation enthalpy.<sup>18</sup> (4) The rate constant correlates with the solvent viscosity  $\eta$  at short distances as  $k_{\text{ET}} \propto \eta^{-\delta}$  with  $\delta \simeq 0.3 - 0.6$ . Some correlation with viscosity is observed for essentially all distances where measurements are possible, up to the tunneling distance of  $\simeq 24 \text{ \AA}$ .<sup>35</sup> The power exponent  $\delta$  decays with increasing the tunneling distance and is essentially zero at the tunneling distances exceeding  $24 \text{ \AA}$ . (5) The activation enthalpy for short distances of electron transfer is strongly affected by the strength of non-specific hydrophobic attachment of the protein to the SAM.<sup>19</sup> Overall, interactions of proteins with SAMs are weak and nonperturbative, preserving both the structure of the monolayer and the redox potential of the protein.<sup>35</sup> The change of pressure implemented in ref 18 does not substantially affect the viscosity of bulk water. The effect of pressure on electron transfer cannot, therefore, be reduced to changes in bulk viscosity and, instead, points to changes in the protein/SAM relaxation. The mean-square displacement of the bound protein, which becomes a key parameter of the theory proposed here, can depend on pressure and lead to the observable pressure effects.

The consensus reached on the basis of experimental studies is that the crossover occurs in the pre-exponential factor of the rate constant  $k_{\text{ET}}$  given by the following general equation

$$k_{\text{ET}} = k_{\text{NA}}/(1 + g) \quad (2)$$

Here, the golden-rule<sup>36</sup> rate constant  $k_{\text{NA}} \propto \Delta$  decays exponentially with the distance  $R$  between the reactant and the electrode,

$$\Delta(R) \propto e^{-\gamma R} \quad (3)$$

where the distance decay parameter  $\gamma$  has a typical value<sup>15,19,37</sup> of  $\gamma \simeq 1 \text{ \AA}^{-1}$ . The subscript “NA”, referring to non-adiabatic, points to a narrower usage of this term often found in the literature.<sup>36</sup> In contrast to a more general definition of non-adiabatic transitions, requiring  $\Delta > k_{\text{B}}T$ ,<sup>29</sup> the realm of the golden rule is often viewed as the limit of non-adiabatic transitions.

1  
2  
3 Since  $k_{\text{NA}} \propto \Delta$  and  $g \propto \Delta$  per eq 1, electronic coupling  $\Delta$  cancels out in the pre-exponential  
4 factor of the rate in eq 2 when  $g > 1$ . The reaction then crosses over to the friction (dynamics)  
5 control of Kramers' reaction kinetics<sup>30</sup>  
6  
7  
8

$$k_{\text{ET}} \propto \tau_x^{-1} \quad (4)$$

9  
10  
11  
12  
13  
14 In this regime, the exponential distance decay of the reaction rate is eliminated and one anticipates a  
15 plateau in the rate's dependence on the distance  $R$ . For this short-distance plateau, one has to addi-  
16 tionally assume  $\tau_x \propto \eta^\delta$  to achieve agreement with the reported scaling of the rate with the solvent  
17 viscosity.<sup>23,35</sup> However, no connection between the Stokes-shift relaxation time  $\tau_x$  and solvent vis-  
18 cosity has been established either theoretically or experimentally. Therefore, eq 4 is incapable of  
19 explaining the viscosity dependence of the reaction rate. The theory presented below resolves this  
20 difficulty.  
21  
22  
23  
24  
25  
26  
27

28 While the concept of frictional control of the reaction rate agrees qualitatively with the majority  
29 of the data, the direct application of eqs 1 and 2 encounters significant difficulties. The reorgani-  
30 zation energy of half redox reaction was recently calculated from simulations of cytochrome *c*  
31 (Cyt-*c*). The value of  $\lambda^r \simeq 0.57$  eV from simulations is in perfect agreement with the analysis  
32 of cyclic voltammetry data.<sup>38,39</sup> In parallel, the relaxation time for the Stokes-shift dynamics was  
33 calculated as  $\tau_x \simeq 300 - 900$  ps in the temperature range 280–360 K. Even though these dynamics  
34 are obviously much slower than the longitudinal polarization dynamics with the relaxation time  
35  $\tau_L \simeq 0.2$  ps used as  $\tau_x$  for homogeneous reactions in water,<sup>24,40</sup> it is still too fast to allow the dy-  
36 namic solvent control according to eq 1. The electronic coupling parameter extracted from fitting  
37 the measured rate turns out to be  $\Delta \sim 10^{-8}$  eV for the SAM thickness in the crossover region. If  
38 this value is combined with  $\tau_x$  from simulations,  $g \simeq 2 \times 10^{-2}$  in eq 2 cannot produce the turnover  
39 to the friction-dominated regime. An effective relaxation time of  $\tau_x \simeq 188$  ns was estimated to  
40 allow the turnover.<sup>12,23</sup> The discrepancy between the typical time-scales of Stokes-shift relaxation  
41 in proteins on the one hand and the requirements to fit the experimental data on the other hand  
42  
43  
44  
45  
46  
47  
48  
49  
50  
51  
52  
53  
54  
55  
56  
57  
58  
59  
60

1  
2  
3 points to a major disconnect between the basic phenomenology reported experimentally and the  
4 theoretical framework used to justify the observations (eqs 1 and 2). The equations offered to re-  
5 solve this contradiction<sup>17,35</sup> are not applicable to the experimental configuration of an immobilized  
6 protein, as we discuss in more detail below.  
7  
8  
9

10  
11 A new theory for the dynamical control of electrochemical reaction rates presented here seeks  
12 to resolve the theory/experiment disagreement in terms of an additional dynamic process affecting  
13 the reaction rate. Oscillations of the protein attached to the SAM-covered electrode via a soft  
14 harmonically restraining potential are considered in addition to the standard polarization dynamics  
15 entering established theories of dynamical control of electron transfer.<sup>24–28,40</sup> Diffusional dynamics  
16 with the diffusion coefficient  $D_R$  modulate the electronic coupling between the reactant and the  
17 electrode on the characteristic length  $\gamma^{-1}$  (eq 3). One therefore anticipates that, in addition to the  
18 Stokes-shift relaxation time  $\tau_x$ , the time-scale related to the dynamics of  $R$  should affect the reaction  
19 rate  
20  
21  
22  
23  
24  
25  
26  
27  
28

$$\tau_\gamma = (\gamma^2 D_R)^{-1} \quad (5)$$

29  
30  
31  
32 The theory presented below indeed finds that this relaxation time appears, under a specific  
33 separation of magnitudes of  $\tau_x$  and  $\tau_\gamma$ , in the pre-exponential factor of the rate constant for the  
34 friction-controlled reactions. In that regime, eq 4 changes to  
35  
36  
37  
38

$$k_{\text{ET}} \propto \tau_\gamma^{-1} \quad (6)$$

39  
40  
41  
42  
43 The range of the friction-controlled regime for the reaction is extended when soft binding of the  
44 protein to the electrode is introduced. The reason is that the parameter  $\Delta$  in eq 1 is replaced with  
45  
46  
47

$$\Delta_e \exp[(3\gamma^2/2)\langle\delta R^2\rangle] \quad (7)$$

48  
49  
50  
51  
52 where  $\Delta_e$  refers to the equilibrium electrode-protein separation and  $\langle\delta R^2\rangle$  is the variance of the pro-  
53 tein displacement in the soft harmonic attachment (we use a short-hand notation,  $\langle\delta R^2\rangle = \langle(\delta R)^2\rangle$ )  
54  
55  
56  
57  
58



1  
2  
3 and  $\langle \delta X^2 \rangle = \langle (\delta X)^2 \rangle$ , for the variances along the coordinates  $R$  and  $X$ , respectively). Increasing  
4  
5  $\langle \delta R^2 \rangle$ , that is allowing softer binding of the protein, broadens the range of parameters (such  
6  
7 as the distance to the electrode) for which the friction-controlled reaction should be observed. In  
8  
9 addition, the mean-square displacement is expected to scale linearly with temperature,  $\langle \delta R^2 \rangle \propto T$ ,  
10  
11 according to the fluctuation-dissipation theorem.<sup>41</sup> This explicit temperature dependence adds a  
12  
13 temperature-dependent component<sup>42</sup> to the activation free energy  $\Delta F^\ddagger(T)$ , which modifies both  
14  
15 the entropy and enthalpy of activation.  
16  
17  
18

## 19 20 21 **Physical model**

22  
23 Models of electron-transfer reactions in solution consider dynamics along two reaction coordinates  
24  
25 bringing the system to the top of the activation barrier: the solvent dynamics and the intramolecular  
26  
27 dynamics. Along these lines, the Sumi-Marcus model,<sup>25</sup> as well as the two-dimensional diffusion  
28  
29 model by Biscout and Szabo,<sup>43</sup> consider the progress of the reacting system along two independent  
30  
31 classical coordinates,  $X$  for the solvent and  $Q$  for intramolecular vibrational motions. Rescaling  
32  
33 of these coordinates,  $X \rightarrow x$  and  $Q \rightarrow q$ , leads to a simple linear condition for the line of the  
34  
35 transition state:  $x + q = \text{Const}$ . The reaction rate is given in terms of the reactive flux across this  
36  
37 line.  
38

39  
40 The situation is somewhat different for electrode reactions. In addition to the polarization co-  
41  
42 ordinate  $x$  and intramolecular coordinates, population dynamics along the distance to the electrode  
43  
44  $R$  describe mass transport. For slow diffusion, the current is dominated by the diffusional mass  
45  
46 transport, while for slow electron transfer it is dominated by the electrode reaction. Even though  
47  
48 diffusional dynamics do not bring the system to the transition state, it nevertheless affects the time  
49  
50 decay of the electrode current in response to a step of the electrode potential.

51  
52 The model adopted here describes an electrochemical experiment in which the reactant (redox  
53  
54 protein) is immobilized at the surface of the electrode and mass transport does not need to be  
55  
56 considered. The reactant is initially in the oxidized (Ox) state, and it accepts the electron from the  
57  
58  
59  
60

metal electrode following a step change of the metal overpotential at  $t = 0$



Our goal is to determine the time evolution of the surface density  $\Gamma(t)$  of the Ox state such that  $\Gamma(0) = \Gamma_0$ .

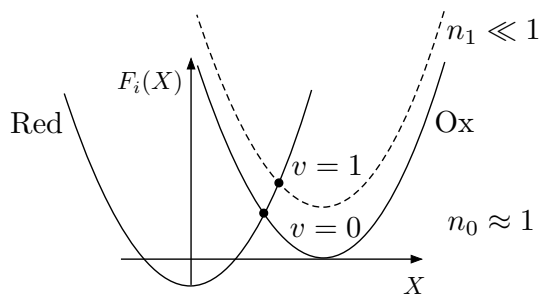


Figure 1: Free energy surfaces  $F_i(X)$  ( $i = \text{Ox}, \text{Red}$ ) of protein electron transfer along the solvent reaction coordinate  $X$  (eq 10). The lower Ox surface indicates the vibrationally ground state  $v = 0$  and the upper Ox state indicates the first vibrationally excited state  $v = 1$ . Since  $n_0 \approx 1$  and  $n_1 \ll 1$ , the vibrationally excited states are not populated for quantum vibrations  $\beta\hbar\omega_v \gg 1$  ( $\beta = (k_B T)^{-1}$ ). Therefore, only the crossing of the lower surfaces with  $v = 0$  contributes substantially to the overall rate in the normal region of electron transfer. The rate is determined by the sum over all vibronic channels (indicated by filled circles) weighted with the corresponding vibrational populations.

The protein is typically bound to the interface either through a surface linker<sup>17</sup> or through a non-specific hydrophobic attachment.<sup>19</sup> In both cases, one can consider binding as a soft harmonic potential with the force constant  $\kappa$  restraining the protein around the equilibrium distance  $R_e$ . For protein electron transfer, the active site is often rigid and does not allow a significant internal reorganization energy (estimated in the range  $\sim 0.05 - 0.09$  eV for Fe-porphins<sup>10,44</sup> and  $\sim 0.1$  eV for azurins<sup>45</sup>). In the case of Cyt-c, the analysis of NMR order parameters for Ox and Red states has indicated a significant rigidity of the protein projecting to a low value of the internal reorganization energy.<sup>46</sup> The rigid structure of the active site also drives the Franck-Condon vibrational modes to the quantum domain. This fact makes even small internal reorganization energy irrelevant for the kinetics. Since most protein redox reactions occur in the electron-transfer normal region,<sup>3</sup> intramolecular reorganization of quantum vibrational modes mostly does not affect the activation barrier of protein electron transfer.<sup>4,47</sup> This is illustrated in Figure 1, which shows that

the vibrationally excited vibronic surfaces need to be populated to allow activated transitions with lower activation barriers. Since populations  $n_v \propto v \exp[-\beta\hbar\omega_v(v + 1/2)]$  of vibronic surfaces with vibrational quantum numbers  $v > 0$  tend to zero for quantum vibrations with  $\beta\hbar\omega_v \gg 1$  ( $\beta = (k_B T)^{-1}$  is the inverse temperature and  $\omega_v$  is the vibrational frequency), there is essentially no contribution of the vibrationally excited states to the reaction rate. The vibrationally excited states of the final (Red) electronic state produce higher activation barriers and also do not contribute. This is what distinguishes the electron-transfer normal region from the inverted region, for which vibrational excitations of the final electronic state (Red in Figure 1) lower the barrier.

The only effect of the quantum modes on the rate in the normal region is to alter the coupling strength  $\Delta'$  to

$$\Delta = \Delta' e^{-S-S_e} \quad (9)$$

Here,  $S = \lambda_v/\hbar\omega_v$  is the Huang-Rhys factor<sup>47,48</sup> determined in terms of the effective vibrational frequency  $\omega_v$  and the vibrational reorganization energy  $\lambda_v$ . An additional quantum correction<sup>49</sup>  $S_e = \mu_e/\hbar\omega_e$  appears from the adiabatic exclusion of the electronic degrees of freedom of the solvent with the characteristic excitation energy  $\omega_e$ ;  $\mu_e$  is the chemical solvation potential of the reactant by these fast degrees of freedom contributing to the electronic polarization of the medium. These quantum Franck-Condon corrections are assumed to be incorporated in the electronic coupling strength  $\Delta$ .

Based on these considerations, we do not need to consider vibrations of the active site and can simplify the model for barrier passage dynamics by assuming that a single reaction coordinate is sufficient to reach the transition state. This reaction coordinate represents thermal fluctuations of the polarizable medium (protein and water) interacting with the charges of the active site. The difference of these Coulomb interactions in the Red and Ox states leads to the reaction coordinate<sup>24,50</sup>

$$X = \int_{\Omega} d\mathbf{r} \delta\mathbf{P} \cdot \Delta\mathbf{E}_0 \quad (10)$$

Here,  $\delta\mathbf{P}$  is the fluctuation of the polarization density out of equilibrium and the integral is taken

over the volume  $\Omega$  occupied by the polarizable medium (protein excluding the active site<sup>51</sup> and water). Further,  $\Delta\mathbf{E}_0$  is the difference of the electric fields of the protein's active site in the final (Red) and initial (Ox) states (including the image effects in the metal electrode).

The variance of  $X$  defines the medium reorganization energy<sup>52</sup>  $\lambda$  through the relation

$$\sigma_x^2 = \langle \delta X^2 \rangle = 2k_B T \lambda \quad (11)$$

This variance reorganization energy should not be confused with the reaction reorganization energy<sup>53</sup>  $\lambda^r$  as explained below. One can further introduce the dimensionless coordinates<sup>25</sup>  $x = X/\sigma_x$  and  $z = \delta R/\sigma_R$ , where  $\delta R = R - R_e$  and

$$\sigma_R^2 = \langle \delta R^2 \rangle = (\beta\kappa)^{-1} \quad (12)$$

The resulting two-dimensional harmonic well is described by the harmonic potential of  $x$  and  $z$

$$\beta V(x, z) = \frac{1}{2}x^2 + \frac{1}{2}z^2 \quad (13)$$

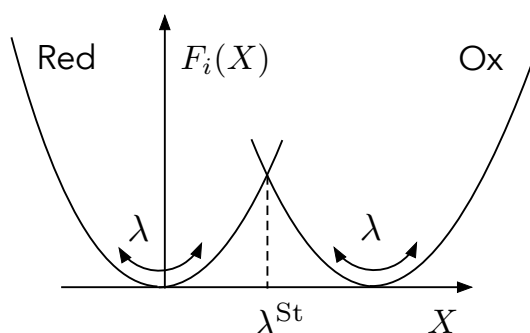


Figure 2: Free energy surfaces  $F_i(X)$  ( $i = \text{Ox, Red}$ ) of protein electron transfer along the reaction coordinate  $X$  (eq 10) reflecting the modulation of the protein electronic states by fluctuations of the medium (protein and water) polarization. The position of the transition state is characterized by the Stokes-shift reorganization energy  $\lambda^{\text{St}}$  and the curvatures of the parabolas are given by variance reorganization energies  $\lambda$  (eq 11). The activation barrier is  $\lambda^r/4$ , where the reaction reorganization energy  $\lambda^r$  is given by eq 15. The configuration shown in the plot corresponds to zero electrode overpotential in electrode reactions.

The free-energy barrier for protein electron transfer is distinct from the rules of the Marcus

theory established for homogeneous electron-transfer reactions in polar solvents. The distinction comes from the fact that sampling of the configuration space by proteins is nonequilibrium (non-ergodic)<sup>4,54</sup> and thus requires two separate reorganization energies,  $\lambda^{\text{St}}$  and  $\lambda$ , for the location of the transition state. This requirement is a special case of a general phenomenology of violation of the fluctuation-dissipation relation<sup>55</sup> in systems out of equilibrium,<sup>56</sup> which also include glassy systems incapable of complete sampling of their phase space.

The relevant parabolic free-energy surfaces along the reaction coordinate  $X$  are illustrated in Figure 2 for a reaction with zero reaction free energy (zero overpotential in electrochemistry<sup>7</sup>). The separation between the parabolas' minima  $X_{0,i}$  is  $2\lambda^{\text{St}} = |X_{0,\text{Ox}} - X_{0,\text{Red}}|$ . Correspondingly, the horizontal distance from the free-energy minimum to the transition state along  $X$  is given by the Stokes-shift reorganization energy  $\lambda^{\text{St}}$ , which carries an analogy to the Stokes shift between absorption and emission maxima for electronic transitions.<sup>53</sup> A separate reorganization energy  $\lambda$  describes the variance of  $X$  or, in other words, the curvature of the parabolas (eq 11). This reorganization energy can be measured from inhomogeneous broadening of optical transition lines.

The change of the perspective from the one dictated by the statistical Gibbs ensemble to the picture of insufficient (nonergodic) sampling does not affect the Marcus energy-gap law, which is based solely on the Gaussian statistics of the energy-gap fluctuations. One therefore obtains for the activation barrier of an electrochemical reaction<sup>4,53</sup>

$$\Delta F^\ddagger = \frac{(\lambda^r + e\varphi)^2}{4\lambda^r} \quad (14)$$

where  $\varphi$  is the electrode overpotential<sup>7</sup> and  $e$  is the elementary charge. However, the definition of the reaction reorganization energy  $\lambda^r$  in terms of the energy-gap reaction coordinate  $X$  changes from  $\lambda = \lambda^{\text{St}} = \lambda^r$  in the Gibbs statistics to<sup>4,53</sup>

$$\lambda^r = (\lambda^{\text{St}})^2 / \lambda \quad (15)$$

specific to nonergodic sampling. Only this parameter, and not  $\lambda^{\text{St}}$  and  $\lambda$  separately, can be reported

1  
2  
3 by the electrochemical experiment.<sup>57</sup> It is easy to see from Figure 2 that the activation barrier at  
4  
5  $\varphi = 0$  becomes

$$6 \quad \Delta F^\ddagger = \frac{X^2}{4\lambda} \Big|_{X=\lambda^{\text{St}}} = \frac{(\lambda^{\text{St}})^2}{4\lambda} = \frac{\lambda^r}{4} \quad (16)$$

10 Even though the two reorganization energies  $\lambda^{\text{St}}$  and  $\lambda$  are not directly accessible by electro-  
11 chemistry, the new definition of the observable reorganization energy  $\lambda^r$  is important since it ex-  
12 plains  $\lambda \gg \lambda^r$  typically produced by numerical atomistic simulations and allows one to reconcile  
13 simulations with experiment. For instance, the experimental value  $\lambda^r \simeq 0.57$  eV for cytochrome  
14 *c* comes from<sup>57</sup>  $\lambda^{\text{St}} = 1.26$  eV and  $\lambda = 2.85$  eV used in eq 15. Equation 15 recovers the standard  
15 theory when full sampling is achieved and  $\lambda^{\text{St}} = \lambda$ . In a general case,  $\lambda^{\text{St}} \leq \lambda$  is required by  
16 thermodynamics.<sup>4</sup>

20 In terms of the scaled reaction coordinate  $x$ , the crossing of the free energy surfaces occurs at

$$24 \quad x_0 = \sqrt{\beta\lambda^r/2} + \phi \quad (17)$$

28 where  $\phi = e\varphi/\sigma_x$  is the scaled value of the electrode overpotential. The transition state  $x_0$  is  
29 achieved by diffusional, overdamped dynamics reflecting the mani-particle thermal fluctuations of  
30 the medium polarization. Each trajectory along the  $x$  coordinate is modified by overdamped diffu-  
31 sion along the coordinate  $z$  modulating the tunneling probability (Figure 3). Concerted fluctuations  
32 of the medium, both bringing the reactant closer to the electrode and shifting its energy level into  
33 resonance with one of the filled electronic states of the metal, are those which provide the highest  
34 values of the electrode current and thus dominate in the reaction rate.

35 With the replacement of the Fermi distribution of the metal electrons with a step function any  
36  $x > x_0$  corresponds to the barrierless tunneling of the electron from the conduction band to the  
37 oxidized state of the reactant. The rate of such transitions is described by the Fermi golden rule as

$$53 \quad k(x, z) = s(z)\theta(x - x_0) \quad (18)$$

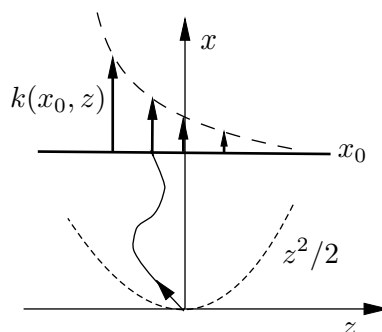


Figure 3: Illustration of the diffusional dynamics in  $(x, z)$  space bringing the system to the transition state  $x_0$  (shown schematically by a single trajectory). The rate of tunneling in the transition state is  $k(x_0, z)$  (eq 18). It exponentially decays with the scaled distance to the electrode  $z = R/\sigma_R$ ,  $\sigma_R^2 = \langle \delta R^2 \rangle$  and is modulated by fluctuations of the reactant's position relative to the electrode. A soft harmonic penalty is imposed on fluctuations along the  $z$ -coordinate.

where  $s(z) = 2\Delta(z)/\hbar$  and  $\theta(x)$  is a Heaviside step function.

The functionality for the tunneling rate adopted here assumes that translations, modulating the tunneling distance, is the main nuclear mode responsible for protein mobility at the surface of the SAM. For proteins immobilized through electrostatic binding, protein rotations become an additional source of thermal noise affecting tunneling.<sup>58</sup> The formalism presented below can potentially apply to these scenarios provided the functional form for the dependence of electronic coupling on the angle of rotation is available and these motions can be projected on harmonic fluctuations of the distance  $R$  to the electrode. In the absence of this functionality, we turn to the mathematical formulation of the present physical model in terms of a two-dimensional stochastic (Fokker-Planck) equation with the population sink specified by eq 18.

## Theory

The overall dynamics of the reactant density  $n(x, z, t)$  is determined by diffusion along the coordinates  $x$  and  $z$  and the sink of the reactant population given through  $k(x, z)$ .<sup>25,59</sup> The diffusional dynamics are described by the corresponding Fokker-Planck equation, which for our purposes is

more convenient to write in the Hamiltonian form

$$\partial_t \bar{n} = - [H + k] \bar{n} \quad (19)$$

Here,  $\bar{n}(x, z)$  is scaled from the original density by the square-root of the equilibrium distribution function

$$\bar{n}(x, z, t) = n(x, z, t) \exp[\beta V(x, z)/2] \quad (20)$$

The Hamiltonian function in eq 19 is easily derived from the Fokker-Planck equation for diffusion in a two-dimensional quadratic potential<sup>60</sup> and is given by the following relation

$$H = H_x + H_z, \quad (21)$$

where

$$H_y = -\tau_y^{-1} \left[ \frac{\partial^2}{\partial y^2} - \frac{y^2}{4} + \frac{1}{2} \right] \quad (22)$$

and  $y = x, z$ . The relaxation time  $\tau_x$  represents Stokes-shift dynamics along the reaction coordinate  $X$  (eq 10) and  $\tau_z = \tau_R = \langle \delta R^2 \rangle / D_R$  is the characteristic diffusion time. We now proceed to solving eq 19 by applying the Sumi-Marcus formalism,<sup>25</sup> which involves an approximate decoupling of certain dynamic correlations in the Green's function for the time evolution of  $\bar{n}(x, z, t)$ .

## Dynamic equation

We adopt the notations by Sumi and Marcus<sup>25</sup> casting the solution of the dynamic evolution equation in terms of bra and ket vectors. Specifically, we will introduce the equilibrium state

$$\langle x, z | e \rangle = [\Gamma_0 / (2\pi)]^{1/2} \exp[-\beta V(x, z)/2] \quad (23)$$



where  $\Gamma_0$  is the equilibrium surface density of the Ox form at the electrode (number of particles per unit area). The normalization of the inner product is obviously

$$\langle e|e\rangle = \Gamma_0 \quad (24)$$

Assuming that the surface density of the reactant is at equilibrium at  $t = 0$ , the evolution of the system described by the ket vector  $|\bar{n}(t)\rangle$  is given by the equation

$$\partial_t |\bar{n}(t)\rangle = -(H + k)|\bar{n}(t)\rangle \quad (25)$$

The ket  $|\bar{n}(t)\rangle$  is defined as

$$\langle x, z|\bar{n}(t)\rangle = (2\pi/\Gamma_0)^{1/2} \bar{n}(x, z, t) \quad (26)$$

This definition results in the initial condition  $|\bar{n}(0)\rangle = |e\rangle$  if equilibrium is assumed at  $t = 0$ :

$$n(x, z, 0) = \Gamma_0/(2\pi) \exp[-\beta V(x, z)] \quad (27)$$

One also obtains the time-dependent surface density  $\Gamma(t)$  by taking the bra-ket

$$\langle e|\bar{n}(t)\rangle = \Gamma(t) \quad (28)$$

By performing the Laplace transform, one gets the equation for Laplace-transformed state  $|\bar{n}(s)\rangle$

$$|\bar{n}(s)\rangle = G(s)|e\rangle \quad (29)$$

where

$$G(s) = [s + H + k]^{-1} \quad (30)$$

is the Green's function (resolvent of the operator  $H + k$ ). The Laplace transform of the dynamic

1  
2  
3 surface density  $\Gamma(t)$  of the Ox state is the matrix element of the Green's function taken with the  
4  
5 equilibrium state

$$6 \quad \Gamma(s) = \langle e | G(s) | e \rangle \quad (31)$$

7  
8  
9  
10 Correspondingly, the electrode current per unit area is obtained by taking the time derivative of the  
11  
12 surface density,  $j(t) = -e d\Gamma(t)/dt$  ( $-e$  is the electron charge). The transient current density can  
13  
14 be Laplace transformed to yield

$$15 \quad j(s) = -e \langle e | sG(s) - 1 | e \rangle \quad (32)$$

16  
17  
18 One can further use the property of the equilibrium states to produce zero eigenvalues,  $H|e\rangle = 0$   
19  
20 and  $\langle e | H = 0$ , to re-write the above equation as

$$21 \quad j(s) = e \langle e | kG(s) | e \rangle \quad (33)$$

22  
23  
24  
25  
26  
27  
28  
29  
30  
31 Equation 33 is formally exact, but cannot be calculated for the sink function given by eq 18.  
32  
33 In order to come up with a closed-form solution, we employ the decoupling ansatz introduced by  
34  
35 Sumi and Marcus.<sup>25</sup> It starts with the exact Dyson equation

$$36 \quad G(s) = G_0(s) - G_0(s)kG(s) \quad (34)$$

37  
38  
39  
40  
41 in which  $G_0(s) = (s + H)^{-1}$  is the Green's function unperturbed by the sink  $k$ . It describes  
42  
43 diffusional dynamics of the system on the two-dimensional harmonic potential. The decoupling of  
44  
45 dynamic correlations in the Sumi-Marcus ansatz consists of projecting out the coupled dynamics  
46  
47 of  $G_0$  and  $G$  on the equilibrium manifold<sup>25</sup> (also see ref 61)

$$48 \quad G_0(s)kG(s) \rightarrow \langle k \rangle^{-1} G_0(s)k|e\rangle \langle e|kG(s) \quad (35)$$

Here

$$\langle k \rangle = \langle e|k|e \rangle \quad (36)$$

is the average rate of the population decay assuming equilibrium distribution of the reactant configurations unperturbed by the reaction dynamics (transition-state theory).

From the decoupling approximation, one immediately obtains a closed-form solution for the Laplace-transformed electrode current density<sup>31</sup>

$$j(s) = e \langle k \rangle [s + sa(s)]^{-1} \quad (37)$$

where

$$a(s) = \langle k \rangle^{-1} \langle e|kG_0(s)k|e \rangle \quad (38)$$

The solution for the dynamics of the electrode current is reduced to the calculation of  $a(s)$ .

## Electrode reaction rate

The main property required for the calculation of the electrode current and the electrochemical reaction rate is the function  $a(s)$  in eqs 37 and 38. It is the Laplace transform of the corresponding time-dependent function

$$A(t) = \langle k \rangle^{-1} \langle e|ke^{-Ht}k|e \rangle \quad (39)$$

The time evolution operator in this equation can be represented by the following bra-ket

$$P(x, z, t; x', z', 0) = \langle x, z|e^{-Ht}|x', z' \rangle \quad (40)$$

which is the well-established propagator of the Ornstein-Uhlenbeck process<sup>60</sup> describing two-dimensional diffusional dynamics in the harmonic potential  $V(x, z)$  given by eq 13. The integrals involved in eq 39 are calculated in the Supporting Information (SI). Here we focus on the results of these calculations leading to closed-form solutions for the electrode current and the rate constant

of electron transfer.

We start with the equilibrium rate of the electrode reaction  $\langle k \rangle$ , which is given by the relation

$$\langle k \rangle = \Gamma_0 k_{\text{NA}} \quad (41)$$

Here, the golden-rule rate of electrode electron transfer is

$$k_{\text{NA}} = \frac{\langle \Delta \rangle}{\hbar} \text{erfc} \left[ \frac{\lambda^r + e\varphi}{\sqrt{4\lambda^r k_{\text{B}} T}} \right] \quad (42)$$

where  $\text{erfc}(x)$  is the complimentary error function.<sup>62</sup> The value of the electronic coupling is averaged over the fluctuation of the protein-electrode distance, which enhance the coupling from the equilibrium value  $\Delta_e$  to the effective coupling<sup>42,63</sup>

$$\langle \Delta \rangle = \Delta_e e^{\gamma^2 \langle \delta R^2 \rangle / 2} \quad (43)$$

Since  $\langle \delta R^2 \rangle \propto T$  according to the fluctuation-dissipation theorem,<sup>41</sup> soft thermally-induced oscillations of the reactant-electrode distance produce temperature-dependent contributions to the enthalpy and entropy of activation.<sup>42</sup>

The time dependent Ornstein-Uhlenbeck propagator entering eqs 39 and 40 depends on two relaxation times,  $\tau_x$  and  $\tau_z$ . This dynamical complexity ensures the complexity of the medium dynamical effect on the rate constant. At large activation barriers,  $x_0^2 \gg 1$ , one can nevertheless arrive at the exponential decay for the electrode current in response to a step of overpotential at  $t = 0$ .<sup>64</sup> As is shown in the SI, the solution is given by the equation<sup>31</sup>

$$j(t) = e\Gamma_0 k_{\text{ET}} e^{-k_{\text{ET}} t} \quad (44)$$

The rate of population decay  $k_{\text{ET}}$  is given by eq 2 with  $k_{\text{NA}}$  from eq 42 and a new definition of the

dynamic crossover parameter  $g$

$$g = \tau_{\text{eff}} \frac{\langle \Delta \rangle}{\hbar} \quad (45)$$

with

$$\tau_{\text{eff}} = 2\tau_{\gamma} e^{\gamma^2 \langle \delta R^2 \rangle} h(\tau_x, \tau_{\gamma}) \quad (46)$$

Here,  $\tau_{\gamma}$  is the characteristic time for translational diffusion over the length of tunneling decay  $\gamma^{-1}$  introduced above (eq 5). This is a new time-scale, which does not appear in the standard formulations of the dynamic effect on electron-transfer kinetics. The appearance of this time-scale is a principal result of this study incorporating protein oscillations modulating the tunneling probability.

The function of two relaxation times  $h(\tau_x, \tau_z) < 1$  in eq 46 has the following analytical form

$$h(\tau_x, \tau_{\gamma}) = 1 - \frac{x_0}{\sqrt{x_0^2 + 4\tau_x/\tau_{\gamma}}} \quad (47)$$

Depending on relaxation times and the harmonic force constants along the two reaction coordinates, it switches between two dynamical regimes. In the limit  $x_0^2 \gg 4\tau_x/\tau_{\gamma}$ , one can take a series expansion of the square root in the denominator in eq 47. The effective relaxation time becomes

$$\tau_{\text{eff}} = \tau_x \frac{8k_{\text{B}}T}{\lambda^r} e^{\gamma^2 \langle \delta R^2 \rangle} \quad (48)$$

Combining this equation with eq 45, one arrives at eq 1 in which  $\Delta$  is replaced with  $\langle \Delta \rangle e^{\gamma^2 \langle \delta R^2 \rangle}$ , where  $\langle \Delta \rangle$  is given by eq 43

$$g = \frac{8\tau_x k_{\text{B}}T \Delta_e}{\hbar \lambda^r} e^{(3\gamma^2/2) \langle \delta R^2 \rangle} \quad (49)$$

Note that accounting for oscillations of the protein relative to the electrode multiplies  $g$  in eq 1 with a large factor of  $\exp[(3\gamma^2/2) \langle \delta R^2 \rangle]$ . This alteration of the dynamic crossover parameter significantly widens the range of friction-controlled electrode kinetics. Obviously, the previous result<sup>31</sup> in eq 1 is restored when  $\langle \delta R^2 \rangle \rightarrow 0$ .

In the opposite limit  $x_0^2 \ll 4\tau_x/\tau_{\gamma}$ , one can drop the second term in eq 47 and put  $h(\tau_x, \tau_z) \approx 1$ .

1  
2  
3 More precisely, for electrode electron transfer from Cyt-c discussed in more detail below, molecular  
4 dynamics simulations have found<sup>57</sup>  $\tau_x(300\text{ K}) \simeq 750\text{ ps}$  and  $\lambda^r \simeq 0.57\text{ eV}$ . In addition, the diffusion  
5 coefficient of Cyt-c in the bulk is<sup>23</sup>  $D_R \simeq 8 \times 10^{-7}\text{ cm}^2\text{s}^{-1}$ . With these estimates and  $\gamma \simeq 1.1$   
6  $\text{\AA}^{-1}$ ,<sup>15</sup> one obtains:  $\tau_\gamma \simeq 100\text{ ps}$ ,  $4\tau_x/\tau_\gamma \simeq 28$  and  $x_0^2 \simeq 11$ . Taken together, these estimates  
7 applied to eqs 46 and 47 lead to

$$\tau_{\text{eff}} \simeq \tau_\gamma e^{\gamma^2 \langle \delta R^2 \rangle} \quad (50)$$

13  
14  
15  
16 As mentioned above, soft harmonic modulation of the distance between protein's active site  
17 and the electrode can be achieved by combined translations and rotations of the protein projected  
18 on the  $z$ -coordinate (Figure 3). Reorientations of the protein electrostatically bound to the SAM  
19 were found to occur on a millisecond time-scale.<sup>22</sup> Therefore,  $\tau_\gamma$  might be affected by combined  
20 rotational-translational dynamics. Keeping in mind that parameters entering eq 45 effectively re-  
21 flect these dynamic complexities, we discuss below electrochemical kinetic data<sup>17</sup> for Cyt-c bound  
22 to the SAM by coordination interactions, when protein translations likely dominate. Many potential  
23 uncertainties in this analysis have been resolved by our recent molecular dynamics simulations of  
24 Cyt-c reporting the reorganization energy of the half reaction and the Stokes-shift relaxation time  
25  $\tau_x$  at a number of temperatures.<sup>57</sup>

## 36 37 38 **Complex dynamics**

39  
40 The variables  $x(t)$  and  $z(t)$  described by Ornstein-Uhlenbeck diffusional dynamics are station-  
41 ary, Gaussian, Markovian stochastic processes characterized by single-exponential time correla-  
42 tion functions with the relaxation times  $\tau_x$  and  $\tau_z$ , respectively. The dynamics of the reaction  
43 coordinates can be multi-exponential or stretched exponential. Accounting for this complication  
44 requires an extension to non-Markovian stochastic processes involving memory functions in the  
45 corresponding Langevin equations.<sup>65</sup> The Langevin equation propagating the stationary, Gaussian,  
46 non-Markovian stochastic process can be transformed into the Fokker-Planck equation for the pop-  
47 ulation dynamics, which gains a time-dependent diffusion coefficient.<sup>65-68</sup> For instance, if one  
48  
49  
50  
51  
52  
53  
54  
55  
56  
57  
58  
59  
60

assumes non-Markovian dynamics along the coordinate  $z$ , eq 22 is generalized to<sup>65</sup>

$$H_z = -\eta_z(t) \left[ \frac{\partial^2}{\partial z^2} - \frac{z^2}{4} + \frac{1}{2} \right] \quad (51)$$

where

$$\eta_z(t) = -\frac{d}{dt} \ln \chi_z(t) \quad (52)$$

is given in terms of the time autocorrelation function  $\chi_z(t) = \langle z(t)z(0) \rangle$ . For a Gaussian stochastic variable, the propagator along the coordinate  $z$  is fully defined<sup>65,67,69,70</sup> in terms of  $\chi_z(t)$

$$\langle z | e^{-H_z t} | z' \rangle \propto \exp \left[ -\frac{(z - z' \chi_z(t))^2}{2(1 - \chi_z(t)^2)} \right] \quad (53)$$

No higher-order time correlation functions are needed to characterize the dynamics.

The long-time Stokes-shift dynamics are typically exponential, as was found in simulations of Cyt-c.<sup>57</sup> Therefore, only the dynamics along the  $z$ -coordinate potentially requires involvement of memory effects in order to account for experimental power-law scaling of the reaction rate with the solvent viscosity.<sup>23,35</sup> As we show in SI, the time-domain function  $A(t) = A(0)F(t)$  in eq 39 can be given by the product of

$$A(0) = \frac{2\langle \Delta \rangle}{\hbar} e^{\gamma^2 \langle \delta R^2 \rangle} \quad (54)$$

and  $F(t) = F_x(t)F_z(t)$  such that  $F(0) = 1$ . The function  $F_x(t)$  is given by eq S20 in SI and does not require modification from the single-exponential, Markovian case. For the function  $F_z(t)$ , the application of the non-Markovian propagator in eq 53 results in

$$F_z(t) = \exp \left[ \gamma^2 \langle \delta R^2 \rangle (\chi_z(t) - 1) \right] \quad (55)$$

The problem of calculating the electrode current is, therefore, reduced to computing the Laplace transform of  $A(t)$  and inverting the Laplace transform of the current in eq 37 to obtain the response to the potential step of the electrode (eq 44).

This procedure leads to a closed-form expression presented in the previous section for the exponential form of  $\chi_z(t)$ , but cannot be accomplished for an arbitrary time correlation function. A separate closed-form solution is, however, possible for the stretched dynamics

$$\chi_z(t) = \exp[-(t/\tau_z)^\delta] \quad (56)$$

with the stretching exponent  $\delta = 1/2$ . This type of stretched dynamics in fact provides a fair account of the conformational dynamics projected on the distance between sites in the protein.<sup>71-73</sup> The main question addressed here is whether the non-Markovian dynamics of the reaction coordinate are projected onto the power-law dependence of the rate on the solvent viscosity. We find that there is no fundamental reason to anticipate this connection. Two limits,  $\tau_{\text{eff}} \propto \tau_x$  and  $\tau_{\text{eff}} \propto \tau_\gamma$ , found for the Markovian dynamics, apply to the non-Markovian dynamics with  $\delta = 1/2$  as well. However, there is a range of parameters for which the power-law dependence on the solvent viscosity can be a reasonable empirical representation of the data.

We show in SI that when  $F_z(t)$  with the correlation function from eq 56 and  $\delta = 1/2$  is used to calculate the current  $j(t)$  (eq 44), one obtains the rate given by eqs 2 and 45 with the effective relaxation time modified from eq 48 to the following relation

$$\tau_{\text{eff}} = \tau_x \frac{8k_B T}{\lambda r} e^{\gamma^2 \langle \delta R^2 \rangle} f(a) \quad (57)$$

with

$$f(a) = \frac{2}{a^2} \left[ \frac{2a}{\sqrt{\pi}} - 2 + (2 - a^2)e^{a^2/4} \text{erfc}(a/2) \right] \quad (58)$$

and

$$a = \frac{2\gamma \sqrt{\langle \delta R^2 \rangle}}{x_0} \sqrt{\frac{\tau_x}{\tau_\gamma}} \quad (59)$$

When the dynamics along the  $z$ -coordinate can be neglected, one has  $a \rightarrow 0$  and  $f(a) \rightarrow 1$ , thus recovering eq 48. On the other hand, when  $a \gg 1$  one gets the asymptote  $f(a) \simeq 4/a^2$  and  $\tau_{\text{eff}} \propto \tau_\gamma$  recovering eq 50. However, in the range of intermediate values of  $a$ ,  $f(a)$  is well approximated by



the equation (Figure S1 in SI)

$$f(a) \simeq (1 + a^{3/2})^{-1} \quad (60)$$

and one obtains at  $a > 1$

$$\tau_{\text{eff}} \propto e^{\gamma^2 \langle \delta R^2 \rangle} \tau_x^{1/4} \tau_\gamma^{3/4} \quad (61)$$

In this range of parameters, a measurement altering  $\tau_\gamma$ , such as by changing the solvent viscosity, will report a power-law dependence on the parameters affecting the relaxation time. However, this calculation strongly suggests that there is no fundamental significance in the power-law dependence of the rate constant on viscosity. Such a mathematical analysis of the data provides a fair representation, in a limited range of parameters,<sup>74</sup> of a more complex functionality, such as that given by function  $f(a)$  in eq 58. In other words, the fact that  $f(a)$  decays with viscosity  $\eta$  slower than  $\propto \eta^{-1}$  does not grant fundamental importance to the power law  $\propto \eta^{-\delta}$ .

## Results

The dependence on the protein-electrode electronic coupling  $\Delta$  disappears from the rate pre-exponential factor in the limit of friction control ( $g > 1$ ) when one gets

$$k_{\text{ET}} = \tau_{\text{eff}}^{-1} \text{erfc} \left[ \frac{\lambda^r + e\varphi}{\sqrt{4\lambda^r k_{\text{B}}T}} \right] \quad (62)$$

This equation can be directly applied to experimental kinetic data for the reduction of Cyt-c attached to the mixed pyridine-terminated alkanthiol PyC<sub>*n*</sub>/C<sub>*n*-1</sub> coating the silver electrode.<sup>17</sup> These kinetic results belong to the plateau region in the dependence of the rate on the SAM thickness. The charge-transfer distance for these SAMs is given in terms of the number  $n$  of methylene groups by the relation:<sup>23</sup>  $R \simeq 1.9 + 1.12n \text{ \AA}$ .

The experimental electron-transfer rates measured<sup>17</sup> by time-resolved surface-enhanced Raman spectroelectrochemistry<sup>22</sup> (TR-SERR) are presented by points in Figure 4. The fact that the rate shows a dependence on the electrode overpotential  $\varphi$ , as expected from standard models of electron

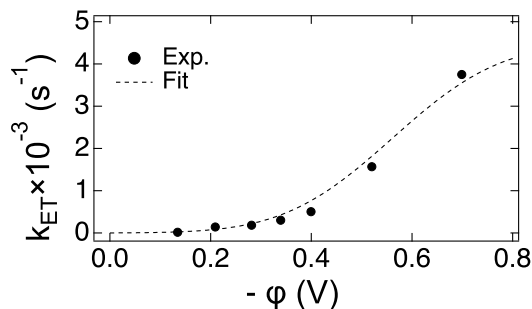


Figure 4: Experimental (Exp.) data for the reduction of Cyt-c<sup>17</sup> on PyC<sub>6</sub>/C<sub>5</sub> SAM coating silver electrode (points),  $T = 298$  K. Shown is the dependence of the electron-transfer rate constant on the electrode overpotential  $\varphi$ . The dashed line is the fit to eq 62 with  $\tau_{\text{eff}} \simeq 0.45$  ms considered as the fitting parameter. The reaction reorganization energy (eq 15),  $\lambda^r(T) = 0.698 - 4.59 \times 10^{-4}T(\text{K})$ , is from molecular dynamics simulations<sup>57</sup> and  $\gamma = 1.12 \text{ \AA}^{-1}$  is adopted to describe the distance falloff of the electronic coupling (eq 3).

transfer,<sup>3</sup> is a strong evidence<sup>22</sup> against the gating mechanism in which a conformational transition of the protein is the rate-limiting step.<sup>21</sup> Indeed, a good fit of the experimental data to eq 62 is possible with  $\tau_{\text{eff}}$  as the single fitting parameter and  $\lambda^r$  taken from molecular dynamics simulations.<sup>57</sup> While the quality of the fit is encouraging, the resulting relaxation time  $\tau_{\text{eff}} \simeq 4.5 \times 10^{-4}$  s is much higher than  $\tau_{\text{eff}} \simeq 188$  ns estimated previously<sup>23</sup> and  $\simeq 370$  ns obtained from our analysis of electrochemical data below. The reasons for the discrepancy between the TR-SERR data and electrochemical kinetics are not entirely clear.<sup>17,58</sup>

Figure 5 shows electrochemical rate constants at  $T = 298$  K reported for PyC<sub>*n*</sub>/C<sub>*n*-1</sub> ( $n = 6, 11, 12, 16$ ) coating gold electrodes (points).<sup>17</sup> The dashed line is the fit to the following equation combining eqs 2, 42, and 45

$$k_{\text{ET}} = \frac{\langle \Delta \rangle / \hbar}{1 + \tau_{\text{eff}} \langle \Delta \rangle / \hbar} \text{erfc} \left[ \frac{\lambda^r + e\eta}{\sqrt{4\lambda^r k_{\text{B}}T}} \right] \quad (63)$$

Fitting the experimental points requires  $\tau_{\text{eff}} \simeq 0.37 \mu\text{s}$  and  $\langle \Delta(n = 11) \rangle = 8.5 \times 10^{-9}$  eV. The fit is done with the fixed  $\gamma = 1.12 \text{ \AA}^{-1}$  while varying  $\tau_{\text{eff}}$  and  $\Delta_0$  in  $\langle \Delta(R) \rangle = \Delta_0 \exp[-\gamma R]$  as two fitting parameters. As above, the reorganization energy is fixed at the value  $\lambda^r \simeq 0.57$  eV from molecular dynamics simulations.<sup>57</sup> If  $\tau_{\gamma} = 10^{-10}$  s estimated above is used in eq 45, the fitted value of  $\tau_{\text{eff}}$  requires the root mean square displacement (rmsd) of the protein relative to the SAM

equal to  $R_{\text{rmsd}} \simeq 2.6 \text{ \AA}$ .

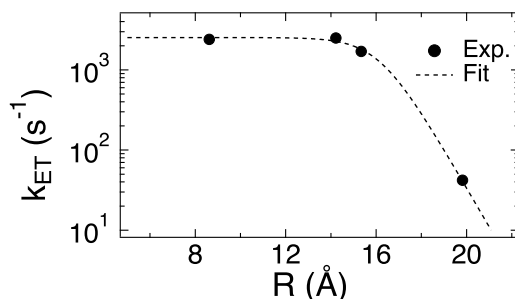


Figure 5: Experimental (Exp.) data for reduction of Cyt-c<sup>17</sup> on PyC<sub>n</sub>/C<sub>n-1</sub> SAM ( $n = 6, 11, 12, 16$ ) coating the gold electrode (points),  $T = 298 \text{ K}$ . The dashed line is the fit to eq 63 with  $\tau_{\text{eff}} \simeq 0.37 \mu\text{s}$ . The rest of the parameters are as in Figure 4.

Observations consistently show<sup>18,19,23,35</sup> an increase of the apparent activation enthalpy for the standard rate constant  $k_0 = k_{\text{ET}}(\varphi = 0)$  in the friction-controlled domain compared to the standard prediction of the Marcus theory,  $\Delta H^\ddagger \simeq \lambda^r/4$ . The increase was attributed to the contribution of the activation energy of the medium relaxation time to the Arrhenius slope. By applying eq 50, one obtains for the standard rate constant at  $\beta\lambda^r \gg 1$  in the friction-controlled region

$$k_0 \approx \frac{1}{\tau_\gamma} \frac{4}{\sqrt{\pi\beta\lambda^r}} e^{-\gamma^2\langle\delta R^2\rangle - \beta\lambda^r/4} \quad (64)$$

If an Arrhenius temperature law is assumed for the relaxation time  $\tau_\gamma = \tau_0 \exp[\beta E_s]$ , one obtains the apparent activation enthalpy

$$\Delta H^\ddagger = \lambda^r/4 + E_s - k_B T \gamma^2 \langle\delta R^2\rangle \quad (65)$$

where the temperature dependences of  $E_s$  and  $\lambda^r$  are neglected and  $\langle\delta R^2\rangle = (\beta\kappa)^{-1}$  (eq 12) was used. Note that  $\lambda^r$  was found to be weakly dependent on temperature in molecular dynamics simulations of Cyt-c.<sup>57</sup>

Along the same lines, one obtains an enhancement of the apparent activation enthalpy in the

regime of the exponential decay of the rate

$$\Delta H_{\text{NA}}^{\dagger} = \lambda^r / 4 + k_{\text{B}} T \gamma^2 \langle \delta R^2 \rangle / 2 \quad (66)$$

The activation enthalpy must be always positive in this regime of the reaction. The second terms in this equation is obviously the activation entropy<sup>42</sup>

$$\Delta S_{\text{NA}}^{\dagger} / k_{\text{B}} = \gamma^2 \langle \delta R^2 \rangle / 2 \quad (67)$$

The appearance of  $E_s$  in eq 65 accounts for an increase of the activation enthalpy in the friction-controlled regime observed experimentally.<sup>18,19,23,35</sup> The last term in eq 65 is reducing this effect, and it is not negligible: according to the fit of the experimental data in Figure 5 it contributes  $\simeq 9k_{\text{B}}T$  to  $\Delta H^{\dagger}$ . Since this term grows with increasing temperature, eq 65 anticipates a possibility of a curved Arrhenius plot. A negative apparent activation enthalpy, producing an anti-Arrhenius slope,<sup>75</sup> can potentially be reached at sufficiently high temperatures.

## Discussion

The present model combines stochastic Kramers' dynamics<sup>30</sup> along the reaction coordinate  $X$  describing the medium polarization<sup>24,50</sup> with the diffusive translational dynamics of the protein in a soft harmonic potential binding it to the electrode. Fluctuations of the protein position modulate the protein-electrode electronic coupling and lead to the appearance of a new characteristic time-scale  $\tau_{\gamma}$  (eq 5) not present in the traditional models of the solvent dynamic effect on electron transfer.<sup>24-28</sup>

Two major outcomes follow from applying the Sumi-Marcus ansatz<sup>25</sup> to calculate the electrode current in response to a step in the electrode potential. First, the relaxation time along the  $R$ -coordinate enters the rate pre-exponential factor:  $\tau_{\gamma}$  replaces  $\tau_x$  appearing in the traditional theories of the dynamic solvent effect.<sup>24-28</sup> Second, the effective relaxation time in eqs 45 and 48 is multiplied by  $\exp[\gamma^2 \langle \delta R^2 \rangle]$ , thus making  $\tau_{\text{eff}}$  significantly higher than the relaxation times of the

1  
2  
3 nuclear fluctuations affecting the barrier passage. This factor comes on the top of a purely sta-  
4 tistical result  $\langle \Delta \rangle = \Delta_e \exp[(\gamma^2/2)\langle \delta R^2 \rangle]$  effectively enhancing the electronic coupling from its  
5 equilibrium value  $\Delta_e$  through protein's translational motions. The overall result is a significant  
6 enhancement of the crossover parameter  $g$  in eq 49 compared to eq 1, where the distance to the  
7 electrode was fixed. A low effective relaxation time required to fit the data was the main source  
8 of disagreement between the traditional theory and observations, which is resolved in the present  
9 formalism. The range of frictional control of the reaction rate is substantially extended compared  
10 to traditional models of the solvent dynamical effect on electron transfer.

11  
12  
13  
14  
15  
16  
17  
18  
19 The analysis of the experimental turnover of the reaction rate with the distance from the elec-  
20 trode (Figure 5) shows that the long relaxation time  $\tau_{\text{eff}}$  required to fit eq 63 can be well accom-  
21 modated if loose binding to the electrode, with  $\text{rmsd} \sim 2 - 3 \text{ \AA}$ , is allowed. Separate studies  
22 are required to establish if this estimate describes the experimental conditions. Comparison with  
23 molecular dynamics simulations<sup>57</sup> shows that  $\tau_{\text{eff}}$  is much longer than the effective time-scale of  
24 Stokes-shift dynamics  $\tau_x \simeq 300 - 900 \text{ ps}$ .

25  
26  
27  
28  
29  
30  
31  
32  
33  
34  
35  
36  
37  
38  
39  
40  
41  
42  
43  
44  
45  
46  
47  
48  
49  
50  
51  
52  
53  
54  
55  
56  
57  
58  
59  
60  
Competition between  $\tau_x$  and  $\tau_\gamma$  time-scales in the rate pre-exponential factor (function  $h(\tau_x, \tau_\gamma)$   
in eq 46) is a result of their close magnitudes:  $\tau_\gamma \sim 100 \text{ ps}$  in our estimates. This situation is very  
different from the relaxation time-scales  $\sim 0.01 - 0.1 \text{ s}$  reported in ref 76. These relaxation times  
represent the dynamics of single-molecule fluorescence life-times of photoexcited flavin adenine  
dinucleotide quenched through electron transfer from a nearby tyrosine electron donor in flavin  
reductase. The mathematical model applied to describe this problem assumed modulation of the  
exponentially decaying tunneling probability by slow donor-acceptor vibrations.<sup>76-78</sup> Their formu-  
lation overlaps with the present agenda considering fluctuations of the protein-electrode distance  
(electrode is the donor and Cyt-c is the acceptor).

If the model of harmonic donor-acceptor fluctuations with the memory friction, similar to the  
one considered here, is adopted,<sup>77</sup> the long time-scales reported in ref 76 require an unreasonably  
high friction of the protein:<sup>72</sup> the friction coefficient from ref 78 is  $\zeta \simeq 20 \text{ g/s}$ , while more re-  
cent direct measurements of the same property have produced<sup>79</sup>  $\zeta \simeq 4 \times 10^{-2} \text{ g/s}$ . This effective

friction is likely to represent population dynamics of the enzyme switching, by overcoming barriers, between active and inactive states<sup>78,80–83</sup> and not necessarily the single-well non-Markovian diffusional dynamics of the variable  $R(t)$ . In our calculations focused on the response current, a much slower relaxation time disappears from the rate and  $k_{\text{ET}} \propto \tau_x^{-1}$  when  $\tau_\gamma \gg \tau_x$ . An additional substantial distinction between the present model and intraprotein distance dynamics studied in ref 76 should be mentioned: the rmsd of the donor-acceptor distance was<sup>78</sup>  $\sim 0.5 \text{ \AA}$  in their case, while a much softer binding of the protein to the SAM, with the rmsd equal to  $\sim 2.6 \text{ \AA}$ , is obtained here from fitting the kinetic data in Figure 5. This large rmsd can be a combined effect of the heterogeneous morphology of the SAM, altering the protein-electrode distance, and of the actual protein-SAM binding (electron tunneling rmsd of  $\simeq 1 \text{ \AA}$  was measured for an osmium complex covalently tethered to alkanethiol SAMs of different length<sup>84</sup>). The heterogeneous component of rmsd does not show up in single-molecule measurements, in contrast to the electrochemical setup.

To complete the discussion, we comment on alternative equations used for the analysis of experiment.<sup>17,35</sup> The rate constant  $k_{\text{ET}}$  derived here describes the decay of the surface population  $\Gamma(t)$  and is therefore expressed in the units of inverse time. Zusman<sup>85</sup> suggested to transform this fixed-distance rate constant to the rate constant  $k_{\text{el}}$  commonly reported for electrode reactions involving mass transport, which has the units of length per time.<sup>7</sup> The transformation is achieved by integrating  $k_{\text{ET}}(R)$  with the assumed uniform bulk distribution of the reactant:  $\rho(R) = \rho_0\theta(R - R_0)$ , where  $\rho_0$  is the bulk concentration. The electrochemical rate constant is then defined as

$$k_{\text{el}}\rho_0 = \int_{R_0}^{\infty} dR \rho(R) k_{\text{ET}}(R) \quad (68)$$

The result of integration in eq 68 with  $k_{\text{ET}}(R)$  from eq 63 is

$$k_{\text{el}} = (\gamma g_0)^{-1} k_{\text{NA}}(R_0) \ln [1 + g_0] \quad (69)$$

where  $g_0 = g(R_0)$  in eq 1 and  $k_{\text{NA}}(R_0)$  is the golden-rule reaction rate in eq 42. This result, assuming a uniform distribution of reactants in solution, does not apply to experiments with reactants

1  
2  
3 attached to the electrode and thus distributed with the one-particle density  $\rho(R) \propto \langle \delta(R - R_e) \rangle$ ,  
4 where the average is over the statistical distribution of  $R$ . It turns out that eq 69 does not apply either  
5 when diffusive mass transport of the reactants to the electrode is allowed. When mass transport is  
6 combined<sup>31</sup> with the Kramers diffusional dynamics in the Sumi-Marcus algorithm, simple volume  
7 integration does not appear in the solution. The dynamics of mass transport, and not the reaction  
8 dynamics, dominate in the electrode current except for the distances closest to the electrode. The  
9 solution given by eq 69 does not, therefore, appear in any problem of practical significance.  
10  
11  
12  
13  
14  
15  
16  
17  
18

## 19 **Concluding remarks**

20  
21  
22 Significant disagreement between experimental data for protein electrochemistry and theoretical  
23 formalisms developed for reactions in solution became apparent when computer simulations al-  
24 lowed for better constraining of the theory parameters and reducing the flexibility of fitting the data.  
25 A theoretical formalism and the analysis of experimental data presented here resolve the theory-  
26 experiment disconnect by introducing a new dissipative mode affecting the rate: overdamped os-  
27 cillations of the protein in a soft harmonic potential binding it to the electrode.  
28  
29  
30  
31  
32  
33

34  
35 Translational dynamics of the protein modulating the electron tunneling probability have been  
36 added to the well-established Kramers-type diffusional dynamics of the medium polarization. Pro-  
37 tein's mobility affects the reaction rate by significantly extending the range of friction-controlled  
38 electrode kinetics. The new model predicts a non-trivial temperature dependence of the activa-  
39 tion enthalpy (eq 65): it can become negative at sufficiently high temperatures producing an anti-  
40 Arrhenius slope when the reaction rate is plotted in the Arrhenius plot vs the inverted temperature.  
41  
42  
43  
44  
45

46  
47 The principle of weak (transient) binding, allowing protein's release after the reaction, is also  
48 realized in biological energy chains, where small redox-active proteins shuttle electrons to larger  
49 membrane-bound protein complexes. The physical mechanisms considered here are, therefore, not  
50 limited to conditions of electrode reactions. The present theory is maintained for charge transfer  
51 between the donor and acceptor connected by a flexible linker or by a binding interaction energy.  
52  
53  
54  
55  
56  
57  
58  
59  
60

1  
2  
3 It predicts that charge transfer will be friction-controlled in a range of donor-acceptor distances and  
4 solvent relaxation times significantly extended for flexible complexes compared to the rigid ones.  
5

6  
7 Similar arguments may apply to intraprotein electron transfer between the donor and acceptor  
8 cofactors within a large protein complex (such as reaction centers of photosynthesis) and, poten-  
9 tially, to hopping charge conductivity in proteins.<sup>86</sup> In all these cases, fluctuations of the distance  
10 between the donor and acceptor sites (hopping sites for conductivity), induced by protein viscoelas-  
11 tic motions, will extend the range of friction-controlled electron transfer. This mechanism will pre-  
12 vent, within certain range of distances, the exponential distance falloff of the charge hopping rate  
13 in complete analogy with the picture shown in Figure 5.  
14  
15  
16  
17  
18  
19  
20  
21  
22

## 23 Acknowledgement

24  
25  
26  
27 This research was supported by the National Science Foundation (CHE-1800243). The author is  
28 grateful to David Waldeck for useful comments on the manuscript.  
29  
30  
31  
32

## 33 Supporting Information Available

34  
35  
36 Derivation of the electrode current in terms of polarization and vibration reaction coordinates (eq  
37 46), derivation of eq 58 for complex dynamics.  
38  
39  
40  
41  
42

## 43 References

- 44  
45  
46 (1) Nicholls, D. G.; Ferguson, S. J. *Bioenergetics 3*; Academic Press: London, 2002.  
47  
48 (2) Warshel, A.; Sharma, P. K.; Kato, M.; Xiang, Y.; Liu, H.; Olsson, M. H. M. Electrostatic basis  
49 for enzyme catalysis. *Chem. Rev.* **2006**, *106*, 3210–3235.  
50  
51  
52 (3) Marcus, R. A.; Sutin, N. Electron transfer in chemistry and biology. *Biochim. Biophys. Acta*  
53 **1985**, *811*, 265–322.  
54  
55  
56  
57  
58  
59  
60



- 1  
2  
3 (4) Matyushov, D. V. Fluctuation relations, effective temperature, and ageing of enzymes: The  
4 case of protein electron transfer. *J. Molec. Liq.* **2018**, *266*, 361–372.  
5  
6  
7  
8 (5) Barbara, P. F.; Meyer, T. J.; Ratner, M. A. Contemporary issues in electron transfer research.  
9  
10 *J. Phys. Chem.* **1996**, *100*, 13148–13168.  
11  
12 (6) Closs, G. L.; Miller, J. R. Intramolecular long-distance electron transfer in organic molecules.  
13  
14 *Science* **1988**, *240*, 440–447.  
15  
16  
17 (7) Bard, A. J.; Faulkner, L. R. *Electrochemical Methods. Fundamentals and Applications*, 2nd  
18 ed.; Wiley: New York, 2001.  
19  
20  
21 (8) Léger, C.; Bertrand, P. Direct electrochemistry of redox enzymes as a tool for mechanistic  
22 studies. *Chem. Rev.* **2008**, *108*, 2379.  
23  
24  
25 (9) Alvarez-Paggi, D.; Hannibal, L.; Castro, M. A.; Oviedo-Rouco, S.; Demicheli, V.; Tórtora, V.;  
26 Tomasina, F.; Radi, R.; Murgida, D. H. Multifunctional cytochrome *c*: Learning new tricks  
27 from an old dog. *Chem. Rev.* **2017**, *117*, 13382–13460.  
28  
29  
30 (10) Winkler, J. R.; Gray, H. B. Electron flow through metalloproteins. *Chem. Rev.* **2014**, *114*,  
31 3369–3380.  
32  
33  
34 (11) Blumberger, J. Free energies for biological electron transfer from QM/MM calculation:  
35 method, application and critical assessment. *Phys. Chem. Chem. Phys.* **2008**, *10*, 5651–5667.  
36  
37  
38 (12) Gray, H. B.; Winkler, J. R. Long-range electron transfer. *Proc. Natl. Acad. Sci.* **2005**, *102*,  
39 3534–3539.  
40  
41  
42 (13) Chidsey, C. E. D. Free energy and temperature dependence of electron transfer at the metal-  
43 electrolyte interface. *Science* **1991**, *251*, 919–922.  
44  
45  
46 (14) Finklea, H. O. Electrochemistry of organized monolayers of thiols and related molecules on  
47 electrodes. *Electroanal. Chem.: A series of advances* **1996**, *19*, 109–335.  
48  
49  
50  
51  
52  
53  
54  
55  
56  
57  
58  
59  
60

- 1  
2  
3 (15) Chi, Q.; Zhang, J.; Andersen, J. E. T.; Ulstrup, J. Ordered assembly and controlled electron  
4 transfer of the blue copper protein azurin at gold (111) single-crystal substrates. *J. Phys. Chem.*  
5 *B* **2001**, *105*, 4669–4679.  
6  
7  
8  
9  
10 (16) Fujita, K.; Nakamura, N.; Ohno, H.; Leigh, B. S.; Niki, K.; Gray, H. B.; Richards, J. H. Mim-  
11 icking protein–protein electron transfer: Voltammetry of pseudomonas aeruginosa azurin and  
12 the thermus thermophilus CuA domain at  $\omega$ -derivatized self-assembled-monolayer gold elec-  
13 trodes. *J. Am. Chem. Soc.* **2004**, *126*, 13954–13961.  
14  
15  
16  
17  
18 (17) Yue, H.; Khoshtariya, D.; Waldeck, D. H.; Grochol, J.; Hildebrandt, P.; Murgida, D. H. On  
19 the electron transfer mechanism between cytochrome *c* and metal electrodes. Evidence for  
20 dynamic control at short distances. *J. Phys. Chem. B* **2006**, *110*, 19906–19913.  
21  
22  
23  
24  
25 (18) Khoshtariya, D. E.; Dolidze, T. D.; Shushanyan, M.; Davis, K. L.; Waldeck, D. H.; van El-  
26 dik, R. Fundamental signatures of short- and long-range electron transfer for the blue copper  
27 protein azurin at Au/SAM junctions. *Proc. Natl. Acad. Sci.* **2010**, *107*, 2757.  
28  
29  
30  
31  
32 (19) Monari, S.; Battistuzzi, G.; Bortolotti, C. A.; Yanagisawa, S.; Sato, K.; Li, C.; Salard, I.;  
33 Kostrz, D.; Borsari, M.; Ranieri, A. et al. Understanding the mechanism of short-range elec-  
34 tron transfer using an immobilized cupredoxin. *J. Am. Chem. Soc.* **2012**, *134*, 11848–11851.  
35  
36  
37  
38  
39 (20) Avila, A.; Gregory, B. W.; Niki, K.; Cotton, T. M. An electrochemical approach to investi-  
40 gate gated electron transfer using a physiological model system: Cytochrome *c* immobilized  
41 on carboxylic acid-terminated alkanethiol self-assembled monolayers on gold electrodes. *J.*  
42 *Phys. Chem. B* **2000**, *104*, 2759–2766.  
43  
44  
45  
46  
47 (21) Jeuken, L. J. C. Conformational reorganisation in interfacial protein electron transfer.  
48 *Biochim. Biophys. Acta - Bioenergetics* **2003**, *1604*, 67–76.  
49  
50  
51  
52 (22) Murgida, D. H.; Hildebrandt, P. Disentangling interfacial redox processes of proteins by SERR  
53 spectroscopy. *Chem. Soc. Rev.* **2008**, *37*, 937–945.  
54  
55  
56  
57  
58  
59  
60

- 1  
2  
3 (23) Waldeck, D. H.; Khoshtariya, D. E. *Applications of Electrochemistry and Nanotechnology in*  
4 *Biology and Medicine I*; Springer New York: New York, NY, 2011; pp 105–238.  
5  
6  
7  
8 (24) Zusman, L. D. Outer-sphere electron transfer in polar solvents. *Chem. Phys.* **1980**, *49*, 295–  
9 304.  
10  
11  
12 (25) Sumi, H.; Marcus, R. A. Dynamical effects in electron transfer reactions. *J. Chem. Phys.* **1986**,  
13 *84*, 4894–4914.  
14  
15  
16 (26) Rips, I.; Jortner, J. Dynamic solvent effects on outer-sphere electron transfer. *J. Chem. Phys.*  
17 **1987**, *87*, 2090–2104.  
18  
19  
20 (27) Hynes, J. T. Outer-sphere electron-transfer reactions and frequency-dependent friction. *J.*  
21 *Phys. Chem.* **1986**, *90*, 3701–3706.  
22  
23  
24 (28) Yan, Y. J.; Sparpagione, M.; Mukamel, S. Solvation dynamics in electron-transfer, isomer-  
25 ization, and nonlinear optical processes: a unified Liouville-space theory. *J. Phys. Chem.*  
26 **1988**, *92*, 4842–4853.  
27  
28  
29 (29) Frauenfelder, H.; Wolynes, P. G. Rate theories and puzzles of hemeprotein kinetics. *Science*  
30 **1985**, *229*, 337–345.  
31  
32  
33 (30) Kramers, H. Brownian motion in a field of force and the diffusion model of chemical reactions.  
34 *Physica* **1940**, *7*, 284–304.  
35  
36  
37 (31) Matyushov, D. V. Potential-step transient response of an electrochemical system. *J. Elec-*  
38 *troanal. Chem.* **1994**, *367*, 1–6.  
39  
40  
41 (32) Schmickler, W.; Santos, E. *Interfacial Electrochemistry*, 2nd ed.; Springer: Berlin, 2010.  
42  
43  
44 (33) Maroncelli, M. The dynamics of solvation in polar liquids. *J. Mol. Liq.* **1993**, *57*, 1–37.  
45  
46  
47  
48 (34) Khoshtariya, D. E.; Dolidze, T. D.; Zusman, L. D.; Waldeck, D. H. Observation of the  
49 turnover between the solvent friction (overdamped) and tunneling (nonadiabatic) charge-  
50  
51  
52  
53  
54  
55  
56  
57  
58  
59  
60

- transfer mechanisms for a  $\text{Au/Fe(CN)}_6^{3-/4-}$  electrode process and evidence for a freezing out of the Marcus barrier. *J. Phys. Chem. A* **2001**, *105*, 1818–1829.
- (35) Zitare, U. A.; Szuster, J.; Scocozza, M. F.; Espinoza-Cara, A.; Leguto, A. J.; Morgada, M. N.; Vila, A. J.; Murgida, D. H. The role of molecular crowding in long-range metalloprotein electron transfer: Dissection into site- and scaffold-specific contributions. *Electrochim. Acta* **2019**, *294*, 117–125.
- (36) Levich, V. G. In *Advances in Electrochemistry and Electrochemical Engineering*; Delahay, P., Ed.; Interscience: New York, 1965; Vol. 4; pp 1–124.
- (37) Newton, M. D.; Smalley, J. F. Interfacial bridge-mediated electron transfer: mechanistic analysis based on electrochemical kinetics and theoretical modelling. *Phys. Chem. Chem. Phys.* **2007**, *9*, 555–572.
- (38) Cheng, J.; Terrettaz, S.; Blankman, J. I.; Miller, C. J.; Dangi, B.; Guiles, R. D. Electrochemical comparison of heme proteins by insulated electrode voltammetry. *Israel J. Chem.* **1997**, *37*, 259–266.
- (39) Wei, J. J.; Liu, H.; Niki, K.; Margoliash, E.; Waldeck, D. H. Probing electron tunneling pathways: Electrochemical study of rat heart cytochrome *c* and its mutant on pyridine-terminated SAMs. *J. Phys. Chem. B* **2004**, *108*, 16912–16917.
- (40) Gayathri, N.; Bagchi, B. Quantum and non-markovian effects in the electron transfer reaction dynamics in the Marcus inverted region. *J. Phys. Chem.* **1996**, *100*, 3056–3062.
- (41) Hansen, J.-P.; McDonald, I. R. *Theory of Simple Liquids*, 4th ed.; Academic Press: Amsterdam, 2013.
- (42) Matyushov, D. V. Electron transfer in molecules with conformational transitions. *Chem. Phys. Lett.* **1993**, *203*, 131–136.

- 1  
2  
3 (43) Bicout, D. J.; Szabo, A. Electron transfer reaction dynamics in non-Debye solvents. *J. Chem.*  
4 *Phys.* **1998**, *109*, 2325–2338.  
5  
6  
7  
8 (44) Sigfriddson, E.; Olsson, M. H. M.; Ryde, U. A comparison of the inner-sphere reorganization  
9 energies of cytochromes, iron-sulfur clusters, and blue copper proteins. *J. Phys. Chem. B* **2001**,  
10 *105*, 5546–5552.  
11  
12  
13  
14 (45) Cascella, M.; Magistrato, A.; Tavernelli, I.; Carloni, P.; Rothlisberger, U. Role of protein  
15 frame and solvent for the redox properties of azurin from *Pseudomonas aeruginosa*. *Proc.*  
16 *Natl. Acad. Sci.* **2006**, *103*, 19641–19646.  
17  
18  
19  
20  
21 (46) Liu, W.; Rumbley, J. N.; Englander, S. W.; Wand, A. J. Fast structural dynamics in reduced  
22 and oxidized cytochrome *c*. *Protein Science* **2009**, *18*, 670–674.  
23  
24  
25  
26 (47) Bixon, M.; Jortner, J. Electron transfer – From isolated molecules to biomolecules. *Adv. Chem.*  
27 *Phys.* **1999**, *106*, 35–202.  
28  
29  
30  
31 (48) Huang, K.; Rhys, A. Theory of light absorption and non-radiative transitions in F-centres.  
32 *Proc. R. Soc. London Ser. A* **1950**, *204*, 406–423.  
33  
34  
35 (49) Matyushov, D. V.; Ladanyi, B. M. Dispersion solute-solvent coupling in electron transfer  
36 reactions. I. Effective potential. *J. Chem. Phys.* **1998**, *108*, 6362–6377.  
37  
38  
39  
40 (50) Warshel, A. Dynamics of reactions in polar solvents. Semiclassical trajectory studies of  
41 electron-transfer and proton-transfer reactions. *J. Phys. Chem.* **1982**, *86*, 2218–2224.  
42  
43  
44 (51) Dinpajoo, M.; Martin, D. R.; Matyushov, D. V. Polarizability of the active site of cytochrome  
45 *c* reduces the activation barrier for electron transfer. *Sci. Rep.* **2016**, *6*, 28152.  
46  
47  
48  
49 (52) Marcus, R. A. On the theory of electron-transfer reactions. VI. Unified treatment for homo-  
50 geneous and electrode reactions. *J. Chem. Phys.* **1965**, *43*, 679–701.  
51  
52  
53 (53) Matyushov, D. V. Protein electron transfer: Dynamics and statistics. *J. Chem. Phys.* **2013**,  
54 *139*, 025102.  
55  
56  
57  
58  
59  
60

- 1  
2  
3 (54) Matyushov, D. V. Protein electron transfer: is biology (thermo)dynamic? *J. Phys.: Condens.*  
4 *Matter* **2015**, *27*, 473001.  
5  
6  
7  
8 (55) Kubo, R. The fluctuation-dissipation theorem. *Rep. Prog. Phys.* **1966**, *29*, 255–284.  
9  
10  
11 (56) Kurchan, J. In and out of equilibrium. *Nature* **2005**, *433*, 222–225.  
12  
13  
14 (57) Seyedi, S.; Waskasi, M. M.; Matyushov, D. V. Theory and electrochemistry of cytochrome *c*.  
15 *J. Phys. Chem. B* **2017**, *121*, 4958–4967.  
16  
17  
18 (58) Ly, H. K.; Martí, M. A.; Martin, D. F.; Alvarez-Paggi, D.; Meister, W.; Kranich, A.; Wei-  
19 dinger, I. M.; Hildebrandt, P.; Murgida, D. H. Thermal fluctuations determine the electron-  
20 transfer rates of cytochrome *c* in electrostatic and covalent complexes. *ChemPhysChem* **2010**,  
21 *11*, 1225–1235.  
22  
23  
24  
25  
26  
27 (59) Tang, J.; Marcus, R. A. Diffusion-controlled electron transfer processes and power-law statis-  
28 tics of fluorescence intermittency of nanoparticles. *Phys. Rev. Lett.* **2005**, *95*, 107401–4.  
29  
30  
31  
32 (60) Gardiner, C. W. *Handbook of Stochastic Methods*; Springer: Berlin, 1997.  
33  
34  
35 (61) Bian, Y.; Wang, Z.; Chen, A.; Zhao, N. Fluctuating bottleneck model studies on kinetics of  
36 DNA escape from  $\alpha$ -hemolysin nanopores. *J. Chem. Phys.* **2015**, *143*, 184908–8.  
37  
38  
39  
40 (62) Abramowitz, M., Stegun, I. A., Eds. *Handbook of Mathematical Functions*; Dover: New  
41 York, 1972.  
42  
43  
44 (63) Borgis, D. C.; Lee, S.; Hynes, J. T. A dynamical theory of nonadiabatic proton and hydrogen  
45 atom transfer reaction rates in solution. *Chem. Phys. Lett.* **1989**, *162*, 19–26.  
46  
47  
48  
49 (64) Henstridge, M. C.; Laborda, E.; Rees, N. V.; Compton, R. G. Marcus–Hush–Chidsey theory  
50 of electron transfer applied to voltammetry: A review. *Electrochim. Acta* **2012**, *84*, 12–20.  
51  
52  
53  
54 (65) Fox, R. F. The generalized Langevin equation with Gaussian fluctuations. *J. Math. Phys.* **1977**,  
55 *18*, 2331–2335.  
56  
57  
58  
59  
60

- 1  
2  
3 (66) Hänggi, P. Correlation functions and masterequations of generalized (non-Markovian)  
4 Langevin equations. *Z. Physik B* **1978**, *31*, 407–416.  
5  
6  
7  
8 (67) Dong, W.; Andre, J. C. Diffusion-controlled reactions. II. An approach based on a generalized  
9 diffusion equation. *J. Chem. Phys.* **1994**, *101*, 299–306.  
10  
11  
12 (68) Chaudhury, S.; Cherayil, B. J. Complex chemical kinetics in single enzyme molecules:  
13 Kramers’s model with fractional Gaussian noise. *J. Chem. Phys.* **2006**, *125*, 024904–10.  
14  
15  
16  
17 (69) Wang, M. C.; Uhlenbeck, G. E. On the theory of the Brownian motion II. *Rev. Mod. Phys.*  
18 **1945**, *17*, 323–342.  
19  
20  
21 (70) Goychuk, I. In *Adv. Chem. Phys.*; Rice, S. A., Dinner, A. R., Eds.; Wiley, 2012; Vol. 150; pp  
22 187–253.  
23  
24  
25  
26 (71) Min, W.; Luo, G.; Cherayil, B. J.; Kou, S. C.; Xie, X. S. Observation of a power-law memory  
27 kernel for fluctuations within a single protein molecule. *Phys. Rev. Lett.* **2005**, *94*, 198302.  
28  
29  
30  
31 (72) Tang, J.; Lin, S.-H. Distance versus energy fluctuations and electron transfer in single protein  
32 molecules. *Phys. Rev. E* **2006**, *73*, 3597–10.  
33  
34  
35  
36 (73) Satija, R.; Das, A.; Makarov, D. E. Transition path times reveal memory effects and anomalous  
37 diffusion in the dynamics of protein folding. *J. Chem. Phys.* **2017**, *147*, 152707–9.  
38  
39  
40  
41 (74) Pressé, S. A data-driven alternative to the fractional Fokker–Planck equation. *J. Stat. Mech.:*  
42 *Theory and Experiment* **2015**, P07009.  
43  
44  
45 (75) Waskasi, M. M.; Gerdenis,; Moore, A. L.; Moore, T. A.; Gust, D.; Matyushov, D. V. Marcus  
46 bell-shaped electron transfer kinetics observed in an Arrhenius plot. *J. Am. Chem. Soc.* **2016**,  
47 *138*, 9251–9257.  
48  
49  
50  
51 (76) Yang, H.; Luo, G.; Karnchanaphanurach, P.; Louie, T.-M.; Rech, I.; Cova, S.; Xun, L.;  
52 Xie, X. S. Protein conformational dynamics probed by single-molecule electron transfer. *Sci-*  
53 *ence* **2003**, *302*, 262–266.  
54  
55  
56  
57  
58  
59  
60

- 1  
2  
3 (77) Kou, S. C.; Xie, X. S. Generalized Langevin equation with fractional Gaussian noise: Subd-  
4 iffusion within a single protein molecule. *Phys. Rev. Lett.* **2004**, *93*, 180603.  
5  
6  
7  
8 (78) Min, W.; English, B. P.; Luo, G.; Cherayil, B. J.; Kou, S. C.; Xie, X. S. Fluctuating enzymes:  
9 Lessons from single-molecule studies. *Acc. Chem. Res.* **2005**, *38*, 923–931.  
10  
11  
12 (79) Wang, Y.; Zocchi, G. The folded protein as a viscoelastic solid. *EPL (Europhysics Letters)*  
13 **2011**, *96*, 18003.  
14  
15  
16  
17 (80) Xie, X. S. Enzyme kinetics, past and present. *Science* **2013**, *342*, 1457–1459.  
18  
19  
20 (81) Engelkamp, H.; Hatzakis, N. S.; Hofkens, J.; De Schryver, F. C.; Nolte, R. J. M.; Rowan, A. E.  
21 Do enzymes sleep and work? *Chem. Commun.* **2006**, *327*, 935–6.  
22  
23  
24 (82) Lin, C.; Sepunaru, L.; Kätelhön, E.; Compton, R. G. Electrochemistry of single enzymes:  
25 Fluctuations of catalase activities. *J. Phys. Chem. Lett.* **2018**, *9*, 2814–2817.  
26  
27  
28 (83) Grossman-Haham, I.; Rosenblum, G.; Namani, T.; Hofmann, H. Slow domain reconfiguration  
29 causes power-law kinetics in a two-state enzyme. *Proc. Natl. Acad. Sci. U.S.A.* **2018**, *115*,  
30 513–518.  
31  
32  
33 (84) Davia, F. G.; Herrera, S. E.; Calvo, E. J. Gaussian distribution of electron transfer distance  
34 in redox terminated self-assembled thiol monolayers. *J. Phys. Chem. C* **2019**, *123*, 13939–  
35 13943.  
36  
37  
38 (85) Zusman, L. D. Outer-sphere electron transfer reactions at an electrode. *Chem. Phys.* **1987**,  
39 *112*, 53–59.  
40  
41  
42 (86) Zhang, B.; Song, W.; Pang, P.; Lai, H.; Chen, Q.; Zhang, P.; Lindsay, S. Role of contacts in  
43 long-range protein conductance. *Proc. Natl. Acad. Sci. USA* **2019**, *116*, 5886–5891.  
44  
45  
46  
47  
48  
49  
50  
51  
52  
53  
54  
55  
56  
57  
58  
59  
60



## TOC Graphic

